Advances in Consumer Research
https://acr-journal.com/
Volume-3 | Issue-2 | Feb 2026
Original Researcher Article

A CFD Analysis of 3-D Turbulent Flow and Heat Transfer Through a Rectangular Duct With Baffles

Rajat Kabiraj[1]*, Ranajit Midya[2], Afzal Hussain[3] and Snehamoy Majumder[4]
[1,2,3]Research Scholar, Department of Mechanical Engineering, Jadavpur University, Kolkata, India
[4]Professor, Department of Mechanical Engineering, Jadavpur University, Kolkata, India

Received: 29/12/2025
Revised: 19/01/2026
Accepted: 31/01/2026
Published: 09/03/2026

ABSTRACT
This study represents numerical simulations of turbulent fluid flow and heat transfer in a rectangular channel equipped with baffles at different geometric orientations. The baffles are positioned in two arrangements: first case on the bottom wall only second case on the bottom and top walls respectively in tandem condition and always normal to the flow direction in each case. The present investigation is focussed to predict the recirculation bubble, reattachment lengths and widths of the separated shear layers, skin friction coefficient and surface Nusselt number etc. in the turbulent flows. The findings are relevant to the general and industrial applications of the flow through a duct with baffles arranged in different orientation. The flow characteristics include path lines, turbulent kinetic energy, velocity vectors, skin friction coefficient, surface Nusselt number etc. These are analysed using the finite volume method with the power-law scheme of S. V. Patankar. The standard $k-\epsilon$ turbulence model with standard wall functions was employed and the SIMPLER algorithm was used for solving pressure-velocity coupling. Simulations were conducted using the commercial ANSYS software along with own code developed. Results indicate that the baffle orientations significantly impact boundary layer separation, recirculation zones and overall thermal performance respectively
Keywords: Rectangular Channel, Baffles, Recirculation, Nusselt Number, Turbulent Flow

INTRODUCTION:

The flow through a rectangular channel represents an important fundamental study in fluid dynamics, with significant implications for various engineering applications particularly with the incorporation of baffles. This fluid flow structure is a pivotal for the understanding and enhancing numerical modelling techniques and is often used as a benchmark for validating computational fluid dynamics models due to its complex features, such as separation, reattachment and turbulence generation respectively. One of the important phenomena associated with flow through a baffled channel is the turbulent reattachment bubble. This process plays a crucial role in numerous real-world applications, including ducts and pipes, flame stabilization in scramjet engines, heat transfer in printed circuit board cooling systems, and multiphase flows in internal combustion engines etc. The effectiveness and efficiency of devices such as diffusers, turbine blades and flow control mechanisms in aerodynamics depend heavily on the control and prediction of flow separation and reattachment.

In duct flows, for instance, baffles are often used to modify flow behaviour to enhance heat transfer, making this an area of active research. Applications include shell-and-tube heat exchangers, cooling panels in aerospace systems and solar air collectors. Baffles promote turbulence, disrupt boundary layers and create reattachment zones, all of which enhance convective heat transfer. When staggered, baffles also induce impingement and cross-wall flow, further boosting heat transfer via increased fluid mixing and wall interaction. In a notable study, Inman [1] analysed convective heat transfer in rectangular channels with internal heat generation, providing insights into turbulent liquid metal flows. These results are applicable to both the thermal entrance and fully developed regions, particularly at moderate Peclet numbers (~100), aiding in estimating local heat transfer coefficients. Sixin Fan et al. [2] developed a low Reynolds number turbulence model tailored to unsteady turbulent boundary layers. This model adapts to near-wall behaviour through functions based on the local turbulent Reynolds number, improving predictions of unsteady skin friction and flow under varying pressure gradients. B. E. Launder et al. [3] Presents the outcome of experimental research on turbulence induced secondary flows in a square section duct. The main emphasis of the experiments has been on the measurement of the secondary flows in a duct with an equally roughed surface. The resultant profiles for smooth and rough surfaces are the same, within the precision of measurement. F.R. Menter [4] proposed two eddy-viscosity turbulence models aimed at improving boundary layer predictions. The baseline (BSL) model uses Wilcox's original formulation near walls, while the Shear-Stress Transport (SST) model modifies eddy-viscosity definitions to enhance performance under adverse pressure gradients, showing improved accuracy in boundary layer resolution. Melling and Whitelaw [5] conducted detailed experimental investigations using laser-Doppler anemometry to measure velocity and turbulence in rectangular ducts. Their work provided enhanced symmetry and more extensive data ranges than earlier studies, with precise measurements of secondary velocity components. Tsan-Hsing Shih et al [6] introduced

a new k-ε eddy viscosity model incorporating reliability constraints in the dissipation equation. This model demonstrated improved accuracy across various flow types, including shear flows and jets, and outperformed standard k-ε models in several configurations. Demuren and Rodi [7] reviewed flow behaviour in non-circular ducts, particularly focusing on turbulence-driven secondary motions. Using forward-marching numerical methods, their work captured essential flow features and turbulence structures in three-dimensional shear layers, consistent with earlier models like those of Naot and Rodi. Thies and Tam [8] explored improvements to the k-ω model by adjusting empirical constants. Their modifications led to improved accuracy in predicting jet flows across a range of Mach numbers (0.4–2.0) and jet temperature ratios (1.0–4.0), applicable to both symmetric and asymmetric configurations. Doormaal and Raithby [9] refined the SIMPLE (Semi-Implicit Method for Pressure-Linked Equations) method originally developed by Patankar and Spalding, simplifying its implementation and reducing computational costs for incompressible flow simulations.

Ekkad and Chinhan [10] conducted experimental studies on two-pass square channels with ribbed walls, using thermochromic liquid crystals to measure local Nusselt number distributions. His findings covered a broad Reynolds number range (6000–60000), offering detailed insights into heat transfer enhancement strategies. Molki and Mostoufizadeh [11] investigated heat transfer in rectangular ducts with staggered baffle arrangements. The presence of baffles significantly increased local and average heat transfer coefficients, especially in the entrance and periodically fully developed regions. These findings provide a basis for optimizing thermal performance in compact heat exchangers. Murata et al. [12] experimented on angled rib turbulators in rotating square ducts and revealed that 60° ribs yielded the highest heat transfer enhancement, particularly in the Reynolds number range of 10,000 to 20,000, emphasizing the impact of rib orientation on thermal behaviour.

Ravi and Vanka [13] utilized Large Eddy Simulation (LES) techniques to study fully developed flow in square ducts. Their analysis at Re = 360 demonstrated the existence of secondary flows and showed that both Reynolds normal and shear stresses significantly contributed to the generation of mean vorticity. Murata and Mochizuki [14] also conducted numerical simulations using second-order finite difference methods to compare laminar (Re = 50) and turbulent (Re = 350) heat transfer distributions. The turbulent case exhibited greater fluid mixing and broader heat transfer zones due to enhanced momentum diffusion. Yang and Shiht [15] applied a modified turbulence model for near-wall flows, using turbulent time and velocity scales to better capture eddy viscosity behaviour, enhancing near-wall prediction fidelity. Moinuddin et al [16] have done experimental studies on turbulent boundary layers over a chine showed symmetrical development and good agreement confirming the quasi-symmetry in streamwise boundary layer evolution.

Husser and Biringen [17] utilized high-order finite difference and spectral methods to solve the Navier-Stokes equations in complex geometries. Their work highlighted near-wall and corner effects in turbulent duct flows using time-splitting numerical integration techniques. Xu and Pollard [18] performed LES-based simulations of flow in square annular ducts. Their grid refinement study revealed the presence of Prandtl's second-kind secondary flows—chains of counter-rotating vortices around duct corners—underscoring the complexity of turbulence in such geometries. Wilcox [19] compared the low-Reynolds number k-ω and k-ε models, finding that the k-ε model struggled with consistency in turbulent boundary layers. In contrast, the k-ω model delivered better accuracy under varying pressure gradients and flow regimes. P. R. Chandra and Alexander [20] evaluated heat transfer and friction in rectangular channels with varying numbers of ribbed walls across Reynolds numbers from 10,000 to 80,000. Their findings contribute to the design of high-performance cooling channels for turbulent internal flows. Present numerical analysis is aimed to understand the complex flow structures related to the rectangular channel with the incorporation of baffles arranged with different configurations.

1 Mathematical formulation

The differential equations governing the turbulent incompressible fluid motion have been represented in this chapter. Subsequently, the numerical modelling for the present work has also been described. Numerical analysis in fluid dynamics involves mathematical representation of the physical problem for which the solution is sought. Essentially, they are the conservation laws of mass, momentum and energy respectively. Following the continuum approach, the governing equations are generated in the form of partial differential equations (PDE). The conservation equation for the mass is referred to as continuity equation while the same for the momentum equation is known as Navier-Stokes equation. Similarly, equations following conservation of energy expressed in terms of temperature.

2 PROBLEM DISCRIPTION

In the figure 1 and figure 2 the schematic geometry of the physical problem has been described. The inlet flow is uniform with constant velocity U_{in}. The walls are fixed and impermeable and a no-slip condition is valid there. The length to rectangular cross section is sufficient to consider a fully developed flow at the outlet. The wall thermal conditions are considered as constant heat wall temperature.

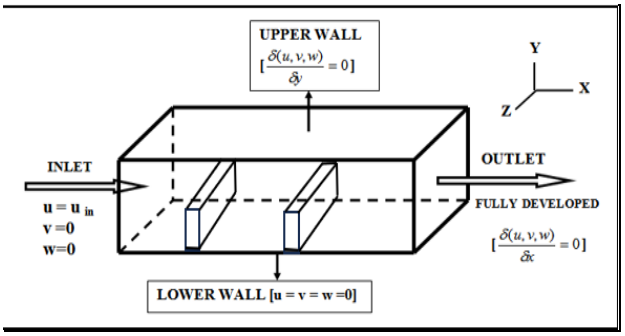

Fig. 1, Physical geometry and flow configuration of the horizontal rectangular duct for inline baffles

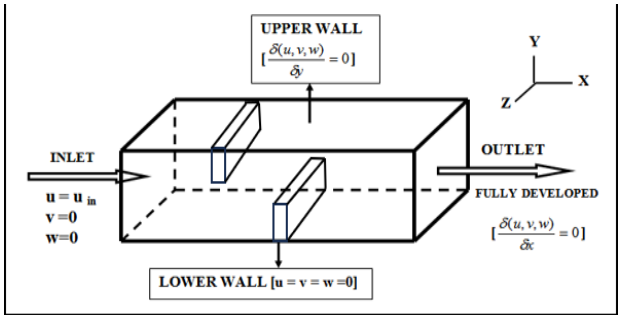

Fig. 2, Physical geometry and flow configuration of the horizontal rectangular duct for staggered baffles

3.1 BOUNDARY CONDITIONS

3.1.1 Velocity boundary condition

At inlet

$u=U_{in}$, $v=0$, $w=0$, $T=T_{in}$

At exit

$\frac{\partial(u,v,w,T)}{\partial x} = 0$, (Pressure boundary conditions may be also given)

At Walls

No-slip boundary condition, i.e. u=v=w=0

$T=T_{wall}$

At Baffles:

No slip boundary condition, i.e., u=v=w=0

$T=T_{baffle}$

3.1.2 Pressure boundary condition

This type of boundary condition is used where boundary values of pressure are known and the exact details of the flow distribution are unknown. This includes pressure inlet and outlet conditions mainly. Typical examples that utilize this boundary condition include buoyancy driven flows, internal flows with multiple outlets, free surface flows and external flows around objects. An example can be of flow outlet into atmosphere where pressure is atmospheric.

3.2 Assumptions

These assumptions are made for the subsequent analysis:

1) The fluid is viscous and incompressible.

2) The flow is steady and turbulent.

3) The geometry is 3-D rectangular with rectangular solid baffles on the top and bottom walls.

4) Uniform -inlet, no-slip wall boundary condition.

4 Governing equations

4.1 Continuity equations

$$\frac{\partial \bar{u}}{\partial x} + \frac{\partial \bar{v}}{\partial Y} + \frac{\partial \bar{w}}{\partial z} = 0 \quad (1)$$

And $$\frac{\partial u'}{\partial x} + \frac{\partial v'}{\partial y} + \frac{\partial w'}{\partial z} = 0 \quad (2)$$

4.2 Reynolds Averaged Navier-Stokes equations:

X-Direction Equation

$$\frac{\partial \bar{u}}{\partial t} + \bar{u}\frac{\partial \bar{u}}{\partial x} + \bar{v}\frac{\partial \bar{u}}{\partial y} + \bar{w}\frac{\partial \bar{u}}{\partial z} = -\frac{1}{\rho}\frac{\partial \bar{p}}{\partial x} + \vartheta\left(\frac{\partial^2 \bar{u}}{\partial x^2} + \frac{\partial^2 \bar{u}}{\partial y^2} + \frac{\partial^2 \bar{u}}{\partial z^2}\right) - \frac{\partial \tau_{xx}}{\partial x} - \frac{\partial \tau_{yx}}{\partial y} - \frac{\partial \tau_{zx}}{\partial z} \quad (3)$$

Y-Direction Equation

$$\frac{\partial \bar{v}}{\partial t} + \bar{u}\frac{\partial \bar{v}}{\partial x} + \bar{v}\frac{\partial \bar{v}}{\partial y} + \bar{w}\frac{\partial \bar{v}}{\partial z} = -\frac{1}{\rho}\frac{\partial \bar{p}}{\partial y} + \vartheta\left(\frac{\partial^2 \bar{v}}{\partial x^2} + \frac{\partial^2 \bar{v}}{\partial y^2} + \frac{\partial^2 \bar{v}}{\partial z^2}\right) - \frac{\partial \tau_{xy}}{\partial x} - \frac{\partial \tau_{yy}}{\partial y} - \frac{\partial \tau_{zy}}{\partial z} \quad (4)$$

Z-Direction Equation

$$\frac{\partial \bar{w}}{\partial t} + \bar{u}\frac{\partial \bar{w}}{\partial x} + \bar{v}\frac{\partial \bar{w}}{\partial y} + \bar{w}\frac{\partial \bar{w}}{\partial z} = -\frac{1}{\rho}\frac{\partial \bar{p}}{\partial z} + \vartheta\left(\frac{\partial^2 \bar{w}}{\partial x^2} + \frac{\partial^2 \bar{w}}{\partial y^2} + \frac{\partial^2 \bar{w}}{\partial z^2}\right) - \frac{\partial \tau_{xz}}{\partial x} - \frac{\partial \tau_{yz}}{\partial y} - \frac{\partial \tau_{zz}}{\partial z} \quad (5)$$

4.3 Energy equation

$$\frac{\partial \bar{T}}{\partial t} + \bar{u}_i\frac{\partial \bar{T}}{\partial x_i} = \frac{\partial}{\partial x_i}\left[\alpha\frac{\partial \bar{T}}{\partial x_i} - \overline{u_i' T'}\right] \quad (6)$$

With

$$-\overline{u_i' T'} = \alpha_t \frac{\partial \bar{T}}{\partial x_i} \quad (7)$$

$$\alpha_t = \vartheta_t / \sigma_t \quad (8)$$

Where σ_t is turbulent prandtl number, $\bar{u}, \bar{v}$ and $\bar{w}$ are the mean velocity components and u', v' and w' are the fluctuating velocity component in the X, Y and Z - directions respectively. $\bar{p}$ is the modified mean pressure; $\bar{T}$ is mean temperature; T' is fluctuating temperature; $\tau_{xx}, \tau_{xy}, \tau_{xz}, \tau_{yy}, \tau_{yz}, \tau_{zz}$ are the component of Reynolds Stress Tensor; ϑ is the kinematic viscosity; ϑ_t is the eddy viscosity; α is the thermal diffusivity and α_t is eddy thermal diffusivity.

Now here as the number of unknowns is more than the number of equations, "the problem is indeterminate" also called in turbulence as "closure problem", one need to close the problem to obtain a solution, for that common turbulence model are classified on the basis of the number of additional transport equations that need to be solved along with RANS Equations

4.4 MODEL EQUATIONS

Here we used Standard K-∈ model to solve these problems along with Continuity equation, RANS Equations and Energy equation.

In the standard K-∈ model with isotropic eddy-viscosity the Reynolds Stress Tensor takes the form: -

The model equation for turbulent kinetic energy, k is

$$\frac{\partial k}{\partial t} + \bar{u}_i\frac{\partial k}{\partial x_j} = \frac{\partial}{\partial x_j}\left[\frac{\vartheta_t}{\sigma_k}\frac{\partial k}{\partial x_j}\right] + P - \epsilon \quad (9)$$

The model equation for turbulent dissipation, ∈ is

$$\frac{\partial \epsilon}{\partial t} + \bar{u}_j\frac{\partial \epsilon}{\partial x_j} = \frac{\partial}{\partial x_j}\left[\frac{\vartheta_t}{\sigma_\epsilon}\frac{\partial \epsilon}{\partial x_j}\right] + C_{\epsilon 1}\frac{P\epsilon}{K} - C_{\epsilon 2}\frac{\epsilon^2}{K} \quad (10)$$

The production of turbulent kinetic, P is

$$P = -\tau_{ij} \frac{\partial \overline{u_i}}{\partial x_k} \quad (11)$$

The entire system of equation can be closed if σ_t is known and ϑ_t is determined correctly. The turbulent viscosity, ϑ_t can be related to turbulent kinetic energy k and its dissipation rate, ϵ in the following way

$$\vartheta_t = C_\mu \frac{K^2}{\epsilon} \quad (12)$$

The quantity C_μ is a model constant to be determined accurately for a specific flow. the kinetic energy k and its dissipation rate ϵ are evaluated at each point in the domain from their governing differential equations.

The standard value of all the model constant as fitted with benchmark experiments are, C_μ=0.09, $C_{\epsilon 1}$=1.44, $C_{\epsilon 2}$ = 1.92, σ_K= 1, σ_ϵ =1.3.

The objective of data reduction is to calculate the average Nusselt number and Reynolds number. The hydraulic diameter, $D_h$is chosen as the characteristic dimension.

$$Re = \frac{UD_h}{\vartheta} \quad (13)$$

$$Nu = \frac{hD_h}{k} \quad (14)$$

Here k is thermal conductivity of flowing fluid.

For rectangular cross-section duct, hydraulic diameter, D_h, is obtained from the following equation.

$$D_h = \frac{4A}{P} \quad (15)$$

Where A is cross-section area and P is wetted perimeter

5. SOLUTION METHODOLOGY

5.1 Numerical algorithm

The mathematical models described above consist of set of differential equations subjected to appropriate boundary conditions. To provide the algebraic form of the governing equations, a fully staggered grid system has been adopted for the velocity components and the scalar variable and these equations wise discretized using a control volume formulation. The numerical solution in present work is accomplished by using Semi implicit method for pressure linked equation revised (SIMPLER) and power-law scheme proposed by Patankar [21].

5.2 Control volume formulation:

In the control volume formulation, the calculation domain is divided into a number of non-overlapping control volumes surrounding each grid point. The differential equation is integrated over each control volume. Piecewise profiles expressing the variation of the variable between the grid points are used to evaluate the required integrals.

The most attractive feature of control volume is that the resulting solution would imply that the integral conservation of quantities such as mass, momentum is exactly satisfied over any group of control volumes, and, of course, over the whole domain. These characteristics exist for any number of grid points. Thus, even the coarse grid solution exhibits exact integral balance.

RESULTS AND DISCUSSION

6.1 Grid Independence Study

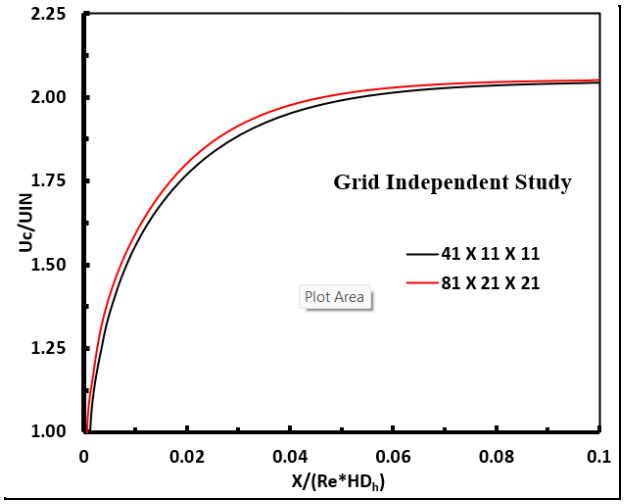

Fig. 3, Grid Independence Study

In the figure 3. The grid independent study has been shown. On the figure we can find that two grid systems of 41×11×11 and 81×21×21 have been used, the results are very closed to each other. So, the result is grid independent. However, we used the grid system of 41×11×11.

6.2 Validation: Nusselt Number Variation with Axial Distance

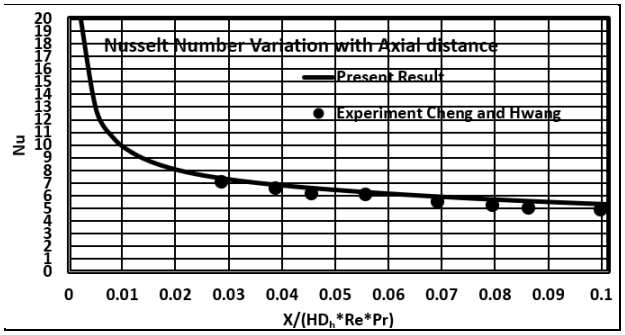

Fig. 4, Validation of the present numerical methods

In the figure 4. The Nusselt Number (Nu) and non-dimensional axial distance X/(HD_h*Re*Pr) have been plotted for present result as well as experimental result Cheng and Hwang [22]. These show the excellent matching of the results. This proved the validation.

6.3 Path lines colour by velocity magnitude:

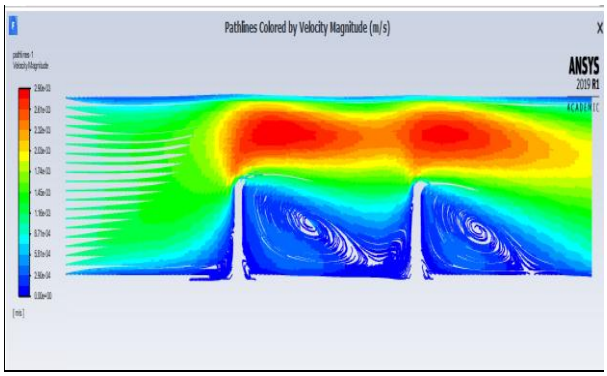

Fig.5, Path lines coloured by velocity magnitude in m/s, for inline baffles, Re = 10000

The path lines coloured by velocity magnitude show distinct flow separation and reattachment patterns behind the backward-facing steps shown in figure 5. High-velocity regions (red) are concentrated in the main stream above the recirculation zones, while low-velocity areas (blue) indicate strong vortex structures within the cavities. The presence of two clear recirculation zones demonstrates the significant impact of step geometry on flow behaviour and momentum distribution.

6.4 Contours of turbulent kinetic energy:

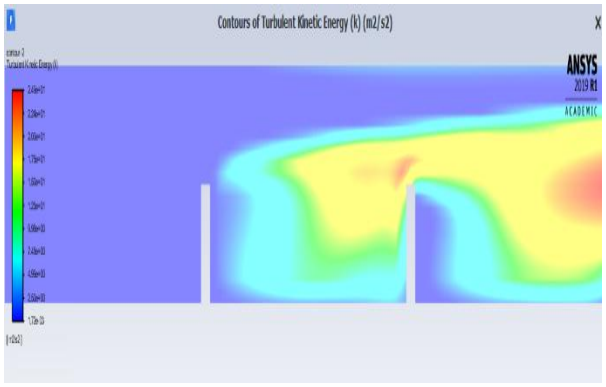

Fig.6, Contours of turbulent kinetic energy for inline baffles, Re = 10000

It is observed from the above figure 6, that turbulent kinetic energy clearly visible after the baffles zone. The contour plot of turbulent kinetic energy (k) reveals elevated turbulence levels immediately downstream of the backward-facing steps. Peak turbulence intensity, shown in red and yellow, occurs near the shear layer where the high-speed core flow interacts with the recirculating zones. The distribution indicates that turbulence generation is closely associated with flow separation and reattachment, gradually diminishing as the flow stabilizes downstream.

6.5 Velocity vectors colour by velocity magnitude:

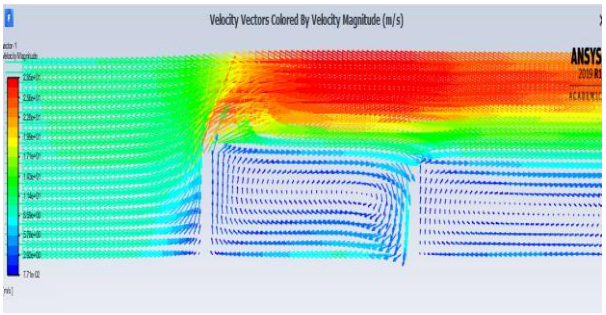

Fig.7, Velocity vectors coloured by velocity magnitude for inline baffles, Re = 10000

The above figure 7, presents the variation of velocity vector around two baffles. The recirculation bubbles around both the baffles are clearly observed in the above figure. A clear recirculation zone is visible immediately downstream of each step, where low-velocity flow (blue) dominates, indicating flow separation and reverse circulation. As the flow progresses downstream, reattachment occurs, and the velocity increases, transitioning from green to red, reflecting higher momentum recovery.

6.6 Path lines colour by velocity magnitude:

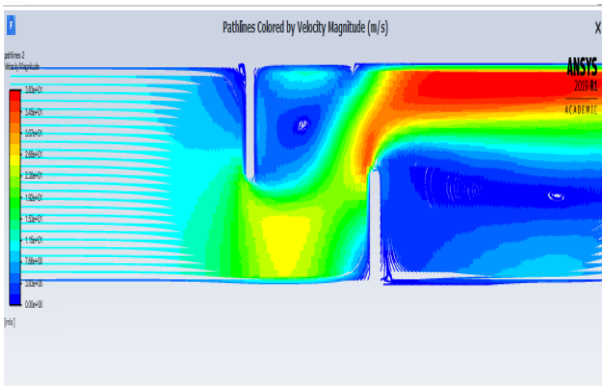

Fig.8, Path lines coloured by velocity magnitude for staggered baffles, Re = 10000

The path line plot shown in the above figure 8, illustrates the velocity distribution in a flow over backward-facing steps, with clear recirculation zones forming behind each step. Low-velocity regions (blue) dominate the recirculation areas, while high-velocity flow (red) remains concentrated in the upper region, indicating bypass of the separated zones. The smooth acceleration and reattachment of the flow suggest a strong influence of step geometry on turbulence development and shear layer formation.

6.7 Velocity vectors colour by velocity magnitude:

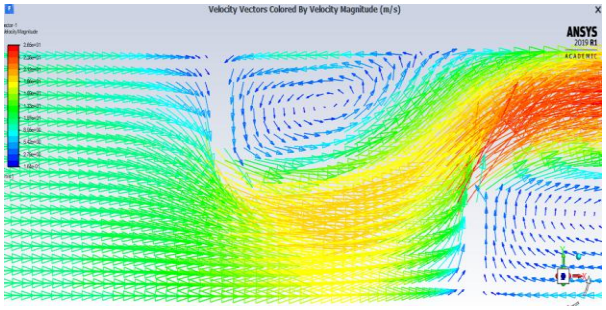

Fig.9, Velocity vectors coloured by velocity magnitude for staggered baffles, Re = 10000

The velocity vector plot highlights a detailed view of the flow separation and reattachment in the vicinity of a backward-facing step shown in figure 9. The region immediately after the step shows a strong recirculation zone with low-velocity vectors (blue), indicating flow reversal. As the flow moves downstream, the velocity magnitude increases (shifting from green to red), and the flow begins to reattach and stabilize. The upper wall exhibits a relatively smooth, high-velocity profile, while the lower wall demonstrates significant interaction with recirculating eddies, affecting local turbulence and heat transfer.

6.8 Skin friction coefficient

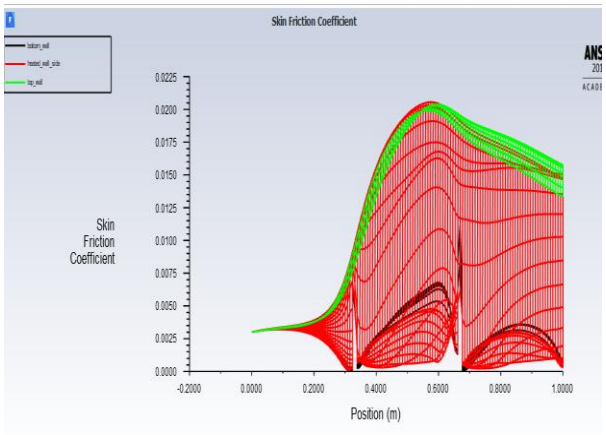

Fig.10, Skin friction coefficient for inline baffles

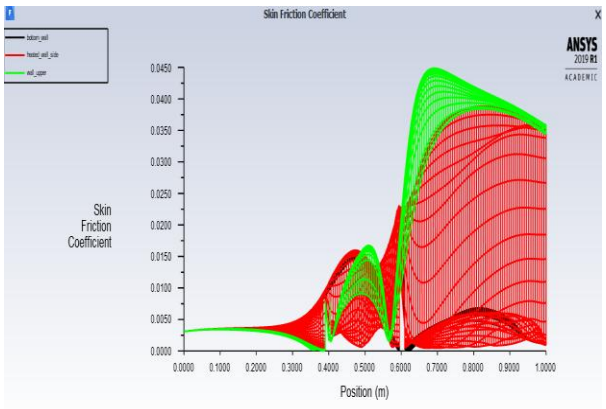

Fig.11, Skin friction coefficient for staggered baffles

The two figures 10 and 11 illustrate the variation of skin friction coefficient along the surface of a model, comparing different wall boundaries: bottom, top/upper, and heated wall side. In the figure 10, the peak skin friction occurs around 0.55 m, with smoother gradients, indicating a relatively stable flow and moderate thermal effects. However, in the figure 11, more pronounced fluctuations and a higher peak skin friction near 0.65 m suggest intensified thermal and flow interactions, likely due to increased heating or altered boundary conditions. The second case also exhibits stronger separation and reattachment zones, as evidenced by sharper oscillations in the red curves. This comparison highlights that thermal loading or surface conditions significantly affect boundary layer behaviour and skin friction development. It is observed from the above two figures that rate of friction is more in case of staggered baffles.

7 Surface Nusselt Number

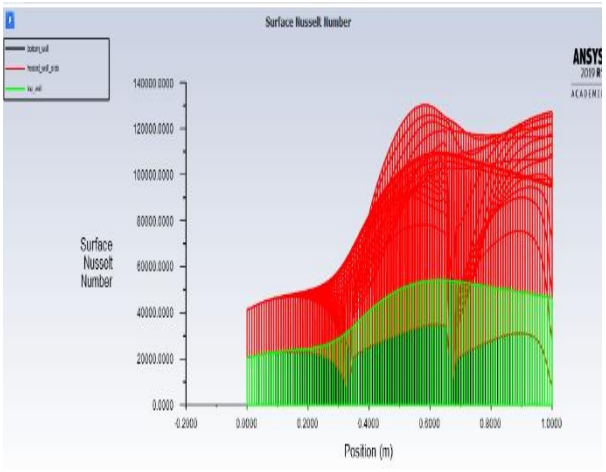

Fig.12, Surface Nusselt Number for inline baffles

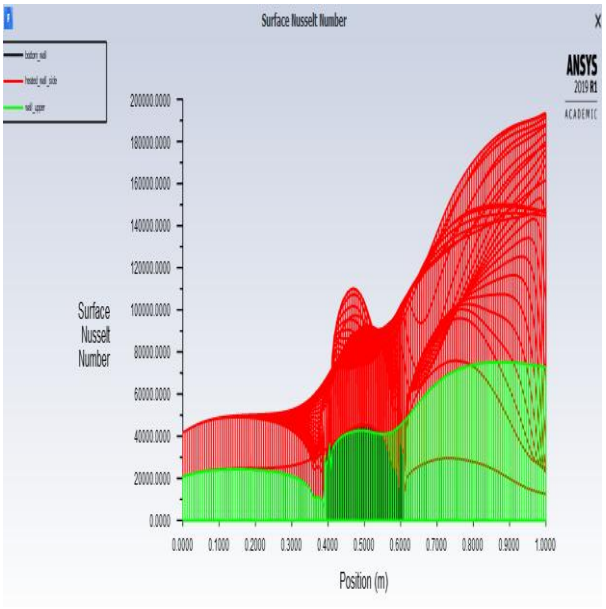

Fig.13, Surface Nusselt Number for staggered baffles

The figures compare the variation of surface Nusselt number along the bottom, top/upper, and heated side walls, highlighting convective heat transfer characteristics. In the figure 12, the heated wall side (red)

shows a peak Nusselt number around 130,000, with smoother progression and gradual increase toward the outlet, indicating more uniform heat transfer. Conversely, the figure 13 shows significantly higher and more irregular Nusselt number spikes on the heated wall, exceeding 190,000, especially between 0.4 m and 0.6 m, suggesting stronger localized thermal gradients or flow disturbances. The top wall in both cases maintains a lower and steadier Nusselt distribution, indicating less influence from direct heating. These differences emphasize that enhanced heat transfer and instability in the second case may be due to intensified thermal loading or geometric or flow modifications. It is observed from the above two figures that rate of heat transfer is more in case of staggered baffles.

CONCLUSION

A numerical analysis of turbulent fluid flow through a 3-D geometry with baffles have been carried out. The effect of the friction, heat transfer and velocity field at the bottom wall, heated side wall and upper wall for a rectangular duct has been observed for both inline and staggered baffles placed across the fluid flow. It is observed from the two cases that rate of heat transfer is more in case of staggered baffles.

.

REFERENCES

1. Robert M. Inman, 1967 'Heat-transfer analysis for liquid-metal flow in rectangular channels with heat sources in the fluid', National aeronautics and space administration, February 1967.
2. Fan, Sixin, Lakshminarayana, Budugur and Barnett Mark, 1993, 'Low-Reynolds-Number k-ϵ Model for Unsteady Turbulent Boundary-Layer Flows', AIAA Journal, October 1993, Vol. 31, No.10.
3. B. E. Launder and W. M. Ying, 1972, 'Secondary flows in ducts of square cross-section', J. Fluid Mech. (1972), vol. 54, part 2, pp. 289-295.
4. Menter F. R., 1994, 'Two-Equation Eddy-Viscosity Turbulence Models for Engineering Applications' AIAA Journal, August 1994, Vol. 32, No. 8.
5. A. Melling and J. H. Whitelaw, 1976, 'Turbulent flow in a rectangular duct, J. Fluid Mech. (1976), vol. 78, part 2, pp. 289-315
6. Tsan-Hsing Shih, William W. Liou, Aamir Shabbir, Zhigang Yang and Jiang Zhu, 1994, 'A new k-ϵ eddy viscosity model for high reynolds number turbulent flows', Computers and Fluids, 1995, Vol. 24, No. 3, pp. 227-238.
7. A. O. Demuren and W. Rodi, 1983, 'Calculation of turbulence-driven secondary motion in non-circular ducts', Fluid Mech. (1984), vol. 140, pp. 189-222.
8. Andrew T. Thies and Christopher K. W. Tam, 1996, 'Computation of Turbulent Axisymmetric and Non axisymmetric Jet Flows Using the k-ϵ Model' AIAA Journal, Vol. February 1996, 34, No. 2.
9. J. P. Van Doormaal and G. D. Raithby,1984, 'Enhancements of the SIMPLE method for predicting incompressible fluid flows', Numerical Heat Transfer,1984 vol. 7, pp. 147-163.
10. Srinath V. Ekkad and JE-Chinhan, 1996, 'Detailed heat transfer distributions in two-pass square channels with rib turbulators', Int. J. Heat Mass Transfer, 1997, Vol. 40, No. 11, pp. 2527-2537.
11. M. Molki and A. R. Mostoufizadeh, 1988, 'Turbulent heat transfers in rectangular ducts with repeated-baffle blockages', Int. J. Heat Mass Transfer. 1989, Vol. 32, No. 8, pp. 1491-1499.
12. Akira Murataa, Sadanari Mochizuki, Tatsuji Takahashi, 1999, 'Local heat transfer measurements of an orthogonally rotating square duct with angled rib turbulators', Columbia International Publishing American Journal of Heat and Mass Transfer, 1999, 42, 3047-3056
13. Ravi K. Madabhushi and S. P. Vanka, 1991 'large eddy simulation on turbulence-driven secondary flow in square duct', Department of Mechanical and Industrial Engineering, University of Illinois at Urbana-Champaign, Urbana, Illinois, 6180I.
14. Akira Murata and Sadanari Mochizuki, 2000, 'Comparison between laminar and turbulent heat transfer in a stationary square duct with transverse or angled- rib turbulators' International Journal of Heat and Mass Transfer, 2001, 44, 1127-1141.
15. Z.Yang and T. H. Shiht, 1993, 'New Time Scale Based $\kappa - \varepsilon$ Model for Near-Wall Turbulence', AIAA JOURNAL, 1993, Vol. 31, No. 7, July.
16. K. A. M. Moinuddin, S,Hafez, P. N. Joubert and M. S. Chong, 2001'Experimental study of turbulent flow along a streamwise edge (chine)' 14th Australasian Fluid Mechanics Conference Adelaide University, Adelaide, Australia, 10-14, December 2001.
17. Asmund Husert and Sedat Biringen, 1993, 'Direct numerical simulation of turbulent flow in a square duct', J. Fluid Mech. (1993), vol. 257, pp. 65-95
18. HongyiXu and Andrew Pollard, 2001, 'Large eddy simulation of turbulent flow in a square annular duct 'American Institute of Physics, VOLUME 13, NUMBER 2001.
19. David C. Wilcox, 1993, 'Comparison of Two-Equation Turbulence Models for Boundary Layers with Pressure Gradient' AIAA JOURNAL, August 1993, Vol. 31, No. 8.

20. P.R. Chandra, C.R. Alexander, J.C. Han, 2003, 'Heat transfer and friction behaviors in rectangular channels with varying number of ribbed walls', International Journal of Heat and Mass Transfer, 2003, 46, 481–495.
21. Patankar, S.V., "Numerical Heat Transfer and Fluid Flow", Hemisphere Publishing Corporation, New York, USA.
22. Y. C. Cheng and G. J. Hawang, 1995, "Experimental Studies of Laminar Flow and Heat Transfer in A One-Porous-Wall Squared Duct with Wall Injection", Int. J. Heat Mass Transfer, Vol. 38, No. 18, pp. 3475-3484
.

.